

Electronic structure and magnetism in UPtAl

A. V. Andreev

Institute of Physics ASCR, Na Slovance 2, 182 21 Prague 8, The Czech Republic

M. Diviš, P. Javorský, K. Prokeš,* and V. Sechovský†

Department of Electron Structures, Charles University, Ke Karlovu 5, 121 16 Prague 2, The Czech Republic

J. Kuneš

Institute of Physics ASCR, Cukrovarnická 10, 160 00 Prague 6, The Czech Republic

Y. Shiokawa

Institute for Materials Research, Tohoku University, Katahira 2-1-1, Aoba-ku, Sendai 980-8577, Japan

(Received 2 March 2001; published 17 September 2001)

Relation between electronic structure and magnetism in UPtAl was studied by *ab initio* band structure calculations in conjunction with several experiments on single crystals focused on magnetic moments (magnetization and neutron-diffraction measurements), magnetic entropy, and anomalous magnetic moment contributions to specific heat and electrical resistivity. The neutron diffraction experiment confirmed the ferromagnetic ordering of U magnetic moments below $T_C=43$ K. The reduced magnetic entropy with respect to the value $R \ln 2$, as derived from specific-heat data, points to a delocalized character of the $5f$ electrons of uranium bearing magnetic moment in this compound. The magnetocrystalline anisotropy in UPtAl is very strong with the anisotropy energy larger than 130 K. In this view, the energies of a gap in magnetic excitation spectrum derived from specific-heat and electrical-resistivity data are unexpectedly low (around 50 K). The electronic structure of UPtAl was calculated in the framework of the local spin density approximation to the density functional theory. The results confirm the large exchange splitting of the uranium $5f$ states which is of the same size as the spin-orbit splitting. The resulting self-consistent charge density is used to discuss the bonding mechanism in UPtAl. Rather large values of the uranium spin $M_S(\text{U})=1.63 \mu_B$ and orbital $M_L(\text{U})=-2.06 \mu_B$ magnetic moment were calculated and compared with the results of previous calculations of Gasche *et al.* Comparison of the total calculated U moment with the values derived both from bulk magnetization measurements and neutron diffraction experiments is discussed as well.

DOI: 10.1103/PhysRevB.64.144408

PACS number(s): 75.30.Cr, 71.20.Lp, 75.30.Gw, 75.40.Cx

I. INTRODUCTION

UPtAl belongs to the ternary UTX compounds (T is a late d -transition element, X is a p element) with the hexagonal ZrNiAl-type crystal structure (the $P\bar{6}2m$ space group). The U ground-state magnetic moment in compounds of this group varies from 0 to $1.6 \mu_B$ depending on the degree of itinerancy of uranium $5f$ electrons. That is determined by the overlap of $5f$ wave functions centered on neighboring U atoms and by the hybridization of $5f$ states with valence electron states of ligands.¹ The latter mechanism usually called the $5f$ -ligand hybridization has been introduced and discussed in various aspects by Koelling *et al.*² The $5f$ -ligand hybridization causes that the T and X atoms affect magnetic properties considerably by influencing the $5f$ -electron states although they do not contribute much to the magnetic moment itself. All the compounds of the group, irrespective of the ground state that can be ferromagnetic (the typical representative is URhAl),^{3,4} antiferromagnetic (UNiAl,⁵ UNiGa¹) or paramagnetic (UCoAl)⁶ exhibit a huge uniaxial magnetic anisotropy.⁷

Magnetization measurements revealed that UPtAl orders ferromagnetically below $T_C=43$ K with a saturated magnetization of $1.38 \mu_B$ per formula unit at 2 K.^{8,9} The strong

uniaxial anisotropy is well demonstrated in Fig. 1 that shows the magnetization curves measured at 4.2 K in magnetic fields applied along the a and c axis. One can see that the c axis is the easy-magnetization direction. In high fields, the magnetic moment is almost saturated at 40 T at a value of $1.49 \mu_B$. The magnetization measured along the a -axis is much smaller without any spontaneous component (in fact, it resembles a magnetic response of a paramagnet exhibiting $0.28 \mu_B/\text{f.u.}$ at 40 T). The crossing point of linearly extrapolated magnetization curves to very high-fields provides a lowest estimated value of the anisotropy field $B_a \approx 290$ T. The corresponding energy of magnetocrystalline anisotropy E_a amounts 130 K in the $k_B T$ representation. Another estimate of anisotropy energy can be derived from the difference between values of the paramagnetic Curie temperature Θ_p , for the c and a axis. For UPtAl this difference $\Delta \Theta_p = 420$ K (Ref. 8) even exceeds the value of the anisotropy energy determined from magnetization measurements in the ordered state.

The shape of virgin magnetization curve in fields applied along the c axis (see inset in Fig. 1) has been preliminary attributed to the coercivity of narrow domain walls in ferromagnetic UPtAl.⁸ Nevertheless, the strong similarity to the virgin magnetization curve of UNiGa, which is an antiferromagnet¹ and shows a sharp metamagnetic transition

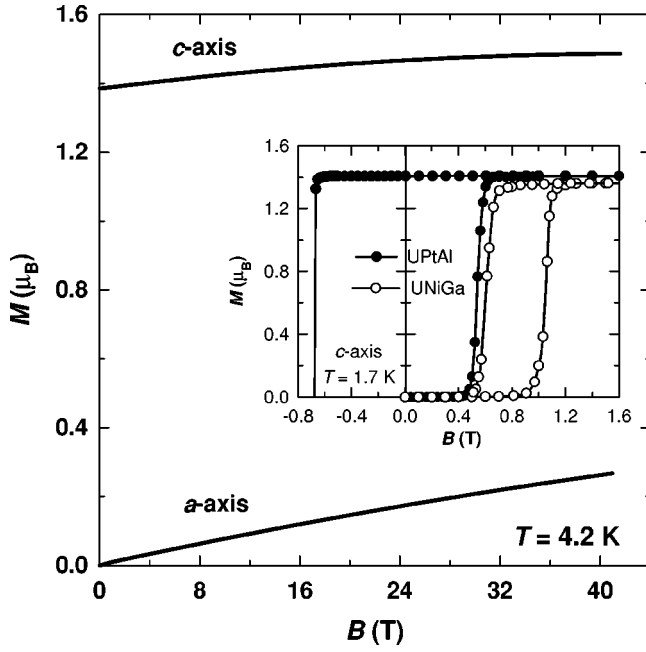


FIG. 1. High-field magnetization curves measured at 4.2 K in fields applied along the a and c axis of the UPtAl single crystal. The inset provides comparison of virgin magnetization curves and hysteresis loops measured at 1.7 K in fields applied along the c axis on single crystals of UPtAl and UNiGa, respectively.

in low fields, may rise some doubts on ferromagnetism in UPtAl. Therefore a neutron-diffraction experiment is strongly desirable to confirm the type of magnetic ground state in this compound.

In this paper we study relation between the electronic structure and magnetism of UPtAl using *ab initio* band structure calculations in conjunction with experiments focused on magnetic moments, magnetic entropy, and anomalous contributions of the system of magnetic moments to specific heat and electrical resistivity. To observe intrinsic properties of this strongly anisotropic ferromagnet all the experiments were performed exclusively on single crystals.

II. EXPERIMENT

Single crystalline samples used for experiments were cut from the main crystal by spark-erosion. The crystal was pulled by a modified Czochralski method in a tetra-arc furnace. The details of the crystal growth are described by Andreev *et al.*⁸

The neutron-diffraction study was performed at the double-axis diffractometer *E4* installed at the Berlin Neutron Scattering Center (BENS) of the Hahn-Meitner-Institute. The crystal was glued onto an aluminum tip with its hexagonal axis parallel to the rotational axis of the diffractometer and inserted into a standard Orange-type cryostat (manufactured by ILL). It was oriented using several sufficiently strong and well centered nuclear reflections and the cell parameters were refined from the UB matrix. The incident neutron wavelength was 2.43 Å.

We have collected two identical sets of integrated intensities, at 2 K and at 65 K. The latter temperature is well

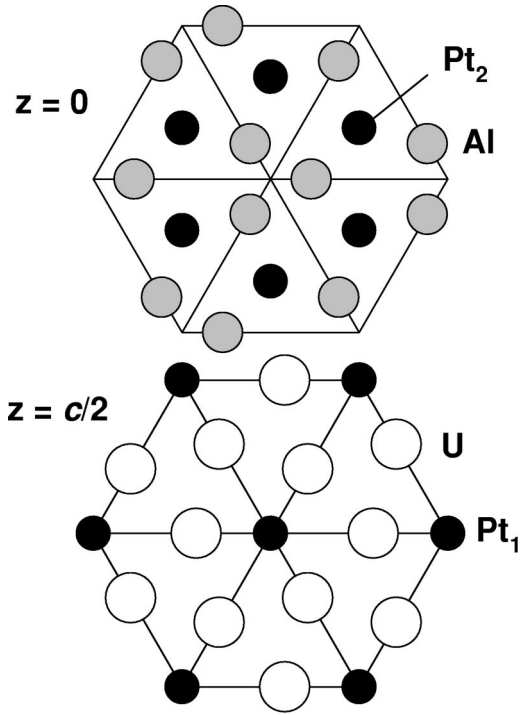


FIG. 2. Hexagonal crystal structure of UPtAl (the ZrNiAl type).

above the Curie temperature ($T_C=43$ K). In addition, we have followed the temperature dependence of the integrated intensity of two reflections in order to confirm the magnetic ordering temperature. The measured ω scans were analyzed by the Lehman-Larson algorithm.¹⁰ The crystallographic and magnetic structures were determined by fitting procedures using the program FULLPROF.¹¹ The values of scattering length were taken from the paper of Sears¹² and the U^{3+} or U^{4+} magnetic form factors in the dipole approximation ($\langle j_0 \rangle + c_2 \langle j_2 \rangle$) from Freeman *et al.*¹³

Magnetization data were obtained in a SQUID magnetometer (Quantum Design) in fields up to 5 T applied along the c axis.

The specific heat was measured by the relaxation method on a 30-mg crystal in the temperature range 2–100 K using the PPMS-14 system (Quantum Design).

III. EXPERIMENTAL RESULTS AND DISCUSSION

A. Neutron diffraction

By refinement of the 65 K data set, we have verified that UPtAl crystallizes in the proper ZrNiAl-type of structure ($P\bar{6}2m$ space group) with lattice parameters $a=701.4$ pm and $c=412.5$ pm that are in satisfactory agreement with the x-ray diffraction data.⁸ This crystal structure of UPtAl is built up by alternating two types of basal-plane atomic layers along the c axis (Fig. 2). One of them contains all of the U atoms and 1/3 of the Pt atoms (the Pt_1 position). The other one consists of the rest of the Pt atoms (the Pt_2 position) together with all of the Al atoms. Each U has four nearest U neighbors within the basal plane and two other neighbors along the c axis. The bonding of the U $5f$ orbitals within the

TABLE I. Structural and magnetic parameters refined by neutron diffraction.

Atom	Site	Local symmetry	Position parameters	$B(\text{\AA}^2)$ $T=65\text{ K}$
U	3(<i>g</i>)	($m2m$)	$x_U\ 0\ 1/2$ $x_U=0.5765(1)$	0.24(2)
Pt ₁	1(<i>b</i>)	($\bar{6}2m$)	0 0 1/2	0.38(1)
Pt ₂	2(<i>c</i>)	($\bar{6}$)	1/3 2/3 0	0.38(2)
Al	3(<i>f</i>)	($m2m$)	$x_{Al}\ 0\ 0$ $x_{Al}=0.2236(3)$	0.64(5)
Cell parameters ($T=65\text{ K}$)		$a=701.4\pm 0.4\text{ pm}$	$c=412.5\pm 0.3\text{ pm}$	
R factors		$R=6.38\%$	$\chi^2=8.45$	
Magnetic moment ($T=2\text{ K}$)		$\mu_U=1.31\pm 0.08\ \mu_B/U$		
R factors		$R_M=11.2\%$	$\chi^2=1.73$	
Curie temperature		42 K		

basal plane together with the strong spin-orbit coupling yields a strong uniaxial magnetocrystalline anisotropy with the easy-magnetization direction along the c axis. The refined structural and magnetic parameters are given in Table I.

At temperatures below T_C , an additional scattering intensity is observed on the top of majority of the Bragg nuclear reflections. Although an effort has been made to detect additional, purely magnetic, reflections by means of typical reciprocal-space scans, no one has been found. This result corroborates the interpretation in terms of ferromagnetic ground state in UPtAl. Temperature dependence of the integrated intensity of (100) reflection, which shows the highest ratio between the magnetic and nuclear intensity, is presented in Fig. 3. The comparison of magnetic intensity with the temperature dependence of the square of spontaneous magnetization in the inset of this figure demonstrates a reasonable agreement between the macroscopic and microscopic magnetic data.

The strong magnetocrystalline anisotropy observed for UPtAl suggests to use Ising model with effective spin $S_{\text{eff}}=1/2$ for the interpretation of our data. We have therefore calculated the temperature dependence of the magnetization using the mean field solution of the Ising model (see Fig. 3, inset). From a comparison of the calculated and experimental data it is clear that such simple mean field solution provides rather poor description of the $M(T)$ data. This suggests that the magnetic excitations, which are driven by the interplay of exchange interactions with the magnetocrystalline anisotropy, can have a quite complex character in UPtAl. This statement is further corroborated by our analysis of specific-heat and resistivity data, and by band structure calculations (see below).

The magnetic structure in UPtAl has been refined from the difference (2–65 K) integrated intensities with a help of the scaling factor inferred from the 65 K data set. When supposing the U^{3+} magnetic form factor, the best agreement has been obtained for a simple collinear ferromagnetic structure of equal U moments of $1.31\pm 0.08\ \mu_B$ oriented along the c axis that is in agreement with magnetization data.^{8,9} We have also performed the same type of refinement supposing

the U^{4+} magnetic form factor. The refined U moment was by about 5% smaller than in the former case while the quality of fits was not changed. This is due to the fact that the magnetic form factors of U^{3+} and U^{4+} are very similar. Clearly, we are not able on the basis of our data to discriminate between the two U valence states.

B. Specific heat

The specific heat data, presented in Fig. 4, show a pronounced anomaly at the ordering temperature $T_C=43\text{ K}$. To

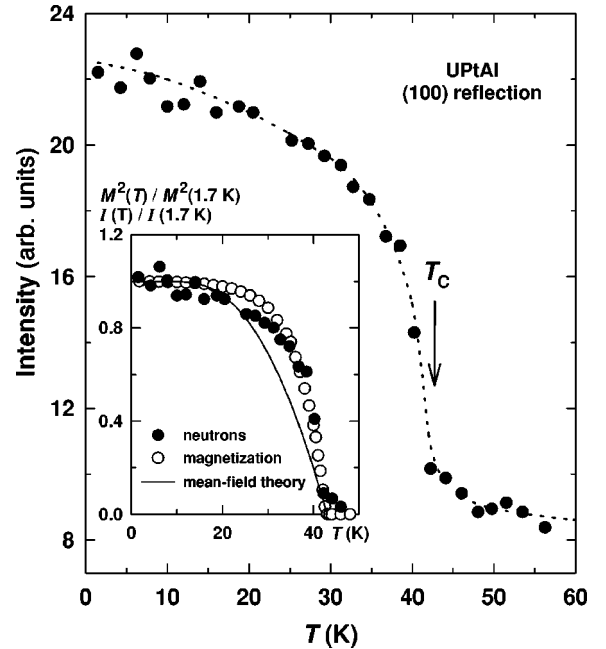


FIG. 3. Temperature dependence of the integrated intensity of the (100) reflection. The inset displays comparison between the reduced neutron-diffraction intensity of the (100) reflection with the square of reduced bulk spontaneous magnetization data. Both quantities were normalized to their lowest temperature values. The full line represents mean field solution of the Ising model.

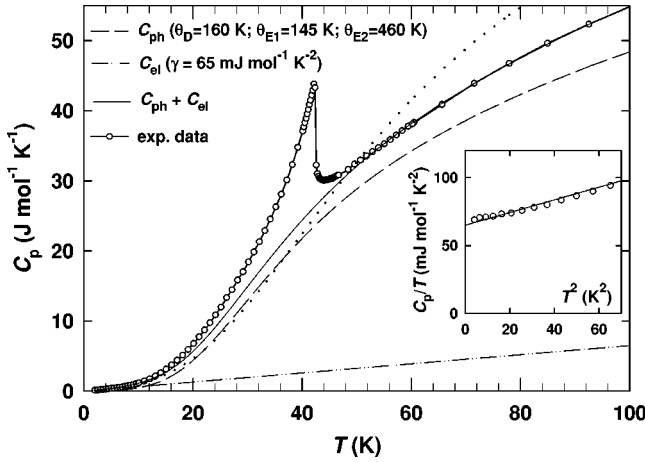


FIG. 4. Temperature dependence of the specific heat of UPtAl. The lines show electronic and phonon contributions as well as their sum. The dotted line represents the nonmagnetic specific heat ($C_{ph} + C_{el}$) when describing all phonon branches by the Debye model ($\theta_D = 240$ K).

analyze these data quantitatively, one has first to estimate the nonmagnetic contribution. It consists of the electronic and phonon parts, C_{el} , and C_{ph} , respectively. The electronic specific heat is expressed by a simple linear temperature dependence

$$C_{el} = \gamma T. \quad (1)$$

For the phonon part, we have assumed the following approximation: the total phonon spectrum consists of 3 acoustic branches, which we describe by the Debye model and characterize by one Debye temperature θ_D , and 6 optical branches, described by the Einstein model and characterized by two different Einstein temperatures θ_E , each describing 3 branches. The phonon contribution can be then calculated by

$$C_{ph} = N_A k_B \left[\sum_j \frac{x_j^2 \exp(x)}{[\exp(x_j) - 1]^2} + 9 \frac{T^3}{\theta_D^3} \int_0^{\theta_D/T} \frac{x^4 \exp(x)}{[\exp(x) - 1]} dx \right]^2, \quad (2)$$

where $x_j = \theta_{Ej}/T$, N_A is the Avogadro number, and k_B is the Boltzmann constant.

Assuming the magnetic specific heat to be negligible at sufficiently low temperatures ($T \ll T_C$), the value of the γ coefficient of C_{el} , $\gamma = 65 \text{ mJ mol}^{-1} \text{ K}^{-2}$, is determined from the low-temperature part of the C_p/T vs T^2 plot (see inset in Fig. 4). The value of θ_D can be then determined by the slope of the C_p/T vs T^2 linear dependence (at $T \ll \theta_D$). Considering three phonon branches described by the Debye model (in the Einstein model, the specific heat is negligible in this temperature range), we obtain $\theta_D = 160$ K. Assuming further $C_{mag} \approx 0$ at $T > T_C$, the measured data above T_C are well described by $\theta_{E1} = 145$ K and $\theta_{E2} = 460$ K. The corresponding calculated specific heat is represented in Fig. 4.

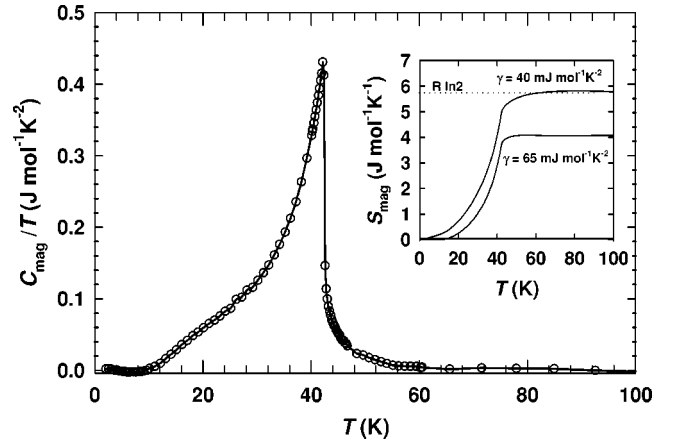


FIG. 5. Temperature dependence of the magnetic contribution to the specific heat of UPtAl. The inset shows temperature dependence of the magnetic entropy supposing different gamma values (see text).

A simple model of the phonon spectrum with all 9 phonon branches described by a single value of $\theta_D = 240$ K within the Debye model has been successfully applied to describe the thermal-expansion data.¹⁴ The value of 240 K is also well comparable with our value of θ_D [$\theta_D = 240$ K describing 9 branches corresponds to $\theta_D = (240/3)^{1/3} \text{ K} = 166$ K for 3 branches]. In Fig. 4 one can see, however, that this simple model fails to describe the C_p data at temperatures above ≈ 50 K and a more complex approximation described above shall be thus used.

The magnetic specific heat, derived from the raw data for the γ and θ values given above, is represented in Fig. 5. It yields a magnetic entropy of $S_{mag} = 4.1 \text{ J mol}^{-1} \text{ K}^{-1} \approx 0.71 R \ln 2$. Although we are aware that the determined value of S_{mag} critically depends on the estimation of C_{el} , and C_{ph} , we can conclude that S_{mag} does not reach the value of $R \ln 2$. The value of $S_{mag} = R \ln 2$ would be obtained, e.g., for $\gamma = 40 \text{ mJ mol}^{-1} \text{ K}^{-2}$ (analysis of C_p above T_C then gives $\theta_D = 160$ K, $\theta_{E1} = 149$ K, $\theta_{E2} = 380$ K) that seems to be nonrealistic (compare to the inset in Fig. 4). Therefore our estimate of S_{mag} provides a strong argument for the delocalized U 5f states in UPtAl. We note that the strong magneto-crystalline anisotropy of UPtAl should also play some role for the magnetic entropy. Note that the value of magnetic entropy determined above is definitely lower than the value $5/3 \ln 2$ that has been derived for isotropic itinerant system.¹⁵

We made an attempt to fit the low-temperature part of C_{mag} first by a commonly used formula describing ferromagnetic spin fluctuations:

$$C_{mag} = a T^3 \ln T, \quad (3)$$

where a is a fitting parameter. As can be seen in Fig. 6, we did not obtain a good agreement with the experimental data in this way. On the other hand, we have found that its low-temperature part fits very well to the formula

$$C_{mag} = a T^{1/2} \exp\left(-\frac{\Delta}{T}\right), \quad (4)$$

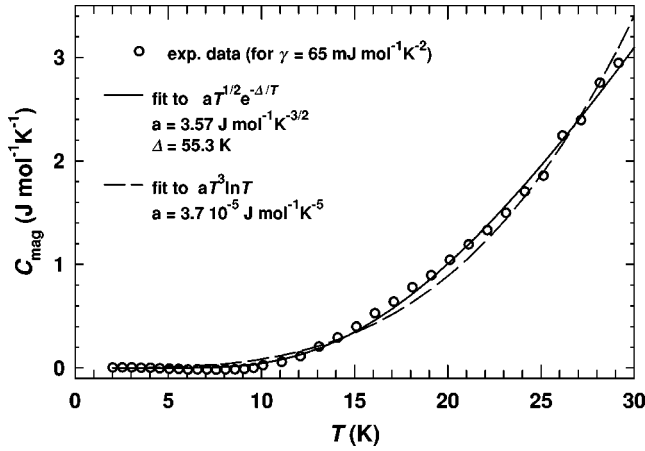


FIG. 6. Fitting curves of the low-temperature magnetic-specific-heat data for UPtAl.

which describes the specific heat of magnons with an energy gap Δ in their dispersion relation.¹⁶ Assuming $\gamma = 65 \text{ mJ mol}^{-1} \text{ K}^{-2}$, the fit of experimental data up to 30 K gives the values of $a = 3.6 \text{ J mol}^{-1} \text{ K}^{-5/2}$ and $\Delta = 55 \text{ K}$ (see Fig. 6). The energy gap Δ derived in this way is, however, rather small in view of the huge magnetic anisotropy of this material.

In this context it is worth to reanalyze data of the electrical resistivity presented by Andreev *et al.*¹⁴ The low-temperature part of the $\rho(T)$ curve can be well fitted with the simple quadratic law:

$$\rho = \rho_0 + aT^2, \quad (5)$$

with $a = 0.047 \text{ } \mu\Omega \text{ cm K}^{-2}$ and $\rho_0 = 59.5 \text{ } \mu\Omega \text{ cm}$. A need of an additional term at higher temperatures is clearly seen in Fig. 7. The contribution of scattering of electrons on

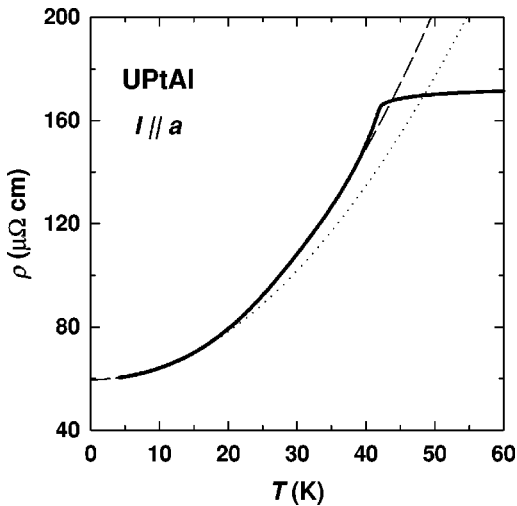


FIG. 7. Temperature dependence of electrical resistivity. The dotted curve shows the fit according to formula (5) with $a = 0.047 \text{ } \mu\Omega \text{ cm K}^{-2}$ and $\rho_0 = 59.5 \text{ } \mu\Omega \text{ cm}$; the dashed curve is the fit of data points up to 39 K according to formula (6) with $a = 0.039 \text{ } \mu\Omega \text{ cm K}^{-2}$, $b = 0.34 \text{ } \mu\Omega \text{ cm K}^{-1}$, $\rho_0 = 59.6 \text{ } \mu\Omega \text{ cm}$, and $\Delta = 27.3 \text{ K}$.

magnon-like excitations can be derived from the mentioned simple model.¹⁶ It leads to the expression

$$\rho = \rho_0 + aT^2 + bT(1 + 2T/\Delta)\exp\left(-\frac{\Delta}{T}\right), \quad (6)$$

the last term accounting for electron scattering on magnetic excitations with a gap Δ . Such term has been identified, e.g., for UNiGe, where $\Delta \approx 40 \text{ K}$,^{1,17} similar to the value obtained from specific heat data. The value of Δ is strongly dependent on the temperature range fitted. Data up to 20 K can be fitted by Eq. (6) for $a = 0.044 \text{ } \mu\Omega \text{ cm K}^{-2}$, $b = 1.45 \text{ } \mu\Omega \text{ cm K}^{-1}$, $\rho_0 = 59.6 \text{ } \mu\Omega \text{ cm}$, and $\Delta = 61.4 \text{ K}$, whereas data up to 39 K lead to $a = 0.039 \text{ } \mu\Omega \text{ cm K}^{-2}$, $b = 0.34 \text{ } \mu\Omega \text{ cm K}^{-1}$, $\rho_0 = 59.6 \text{ } \mu\Omega \text{ cm}$ and $\Delta = 27.3 \text{ K}$. These values certainly compare with the Δ value derived from the specific-heat results. In both cases, however, the value of Δ is too low in comparison with the energy of magnetocrystalline anisotropy estimated from the magnetization and susceptibility data.

This disagreement may be connected with the fact that both the specific heat and resistivity are properties arising from integration over the whole (or at least a large segment) of the Fermi surface.

IV. BAND-STRUCTURE CALCULATIONS

To obtain direct information about the ground-state electronic structure and related properties we also applied first principles theoretical methods. The ground-state electronic structure was calculated on the basis of the density functional theory (DFT) within the local spin density approximation (LSDA).¹⁸ For this purpose we used the full potential linearized augmented plane wave method (LAPW) as implemented in the latest version (WIEN97) of the original WIEN code.¹⁹ The spin-orbit coupling is treated by the second variational step within this implementation. The calculations were performed with the following parameters. The nonoverlapping atomic sphere radii of 148, 132, and 127 pm were taken for U, Pt, and Al, respectively. The basis for expansion of the valence states (less than 6 Ry below Fermi energy) consisted of more than 1000 basis functions (more than 100 APW/atom) plus the U (6s, 6p), Pt (5p), and Al (2p) local orbitals. The uranium 5f states were also treated as the valence Bloch states and thus uranium is characterized by a noninteger occupation number. The Brillouin-zone integrations were performed with the tetrahedron method¹⁹ on a 35–105 special k -points mesh. In order to identify the contributions of individual bands to the orbital moment, within the computer code AVERX we developed a new subroutine for calculating the energy decomposition of the orbital moment.

The total density of electronic states (DOS) and site projected DOS from scalar relativistic non-spin-polarized calculations are shown in Fig. 8. The lowest band that is about -8 to -6 eV originates from the Al 3s states. The Pt 5d states form the main contribution in the energy range -6 to -4 eV (“5d band”) but they show an admixture of the

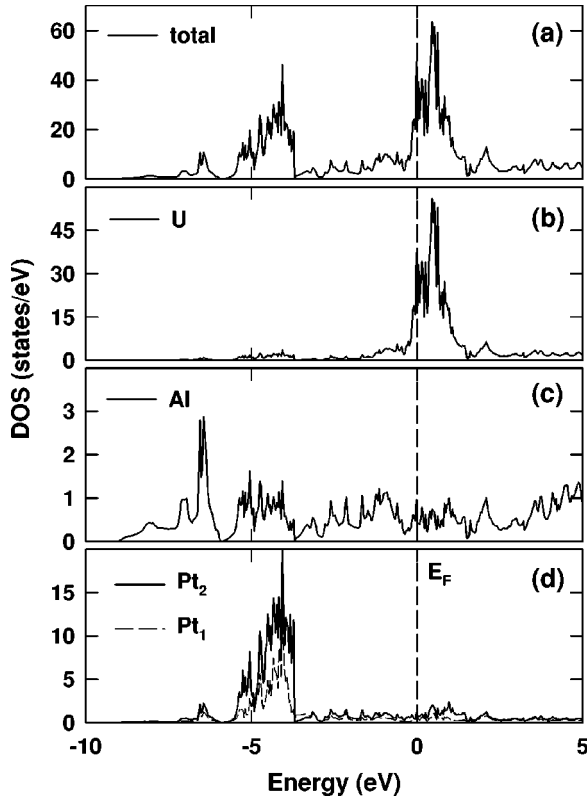


FIG. 8. Calculated scalar relativistic total (a) and site projected nonmagnetic DOS curves [(b), (c), and (d)] in states per hexagonal unit cell of UPtAl. The Fermi energy is set to zero energy.

uranium $7s$, $6d$ states, platinum $6s$ states, and aluminum $3s$, $3p$ states. The highest occupied bands (between -4 and -0.2 eV) originate mainly from the hybridized uranium $5f$ states and platinum $5d$ states but all the remaining (U $7s$, $6d$ states; Al $3p$ states) are also present. Finally we see that the Fermi level is situated inside the U $5f$ band with a rather large DOS. The main part of the U- $5f$ band is only partially occupied and the total bandwidth is roughly 1 eV. The total DOS is in good overall agreement with earlier calculations performed by linear muffin-tin orbital method (LMTO) in the atomic-sphere approximation (ASA) for the description of the effective single electron DFT potential.²⁰ Some differences have been found in the energy region from -0.3 eV to the Fermi level. In this range the DOS values are higher and have different structure than those obtained by the LMTO-ASA method.²⁰

The important results concerning the uranium- f and platinum- d bonding in UPtAl are contained in Table II, which shows the charge distribution over the atomic spheres and its orbital decomposition. Although the Pt $5d$ bands are filled with the Fermi energy lying in the region of U $5f$ bands, the Pt- $5d$ and U- $5f$ occupation numbers are 7.535 (Pt_1), 7.547 (Pt_2), and 2.461 (U), respectively. This is a consequence of the hybridization between the Pt- $5d$ and U- $5f$ states. The region of the rather low DOS (-3 eV $< E < 0.5$ eV) between the U $5f$ and Pt $5d$ derived bands is determined mainly by the energy difference between the corresponding atomic levels and the strength of the U $5f$ -Pt $5d$ hybridization. When we compare the converged ground-state density with that of the simple superposition of neutral atomic charge densities, which is the initial charge density in the Kohn-Sham equations, we find a small charge transfer from the uranium and aluminum to the both platinum sites. Moreover from our band calculations it is now strongly suggested that uranium valency $3+$ or $4+$ cannot have reasonable meaning in the case of UPtAl. This fact corresponds with results of our analysis of neutron diffraction data, which shows that the assumed valency $3+$ or $4+$ has only a negligible effect on the refined value of total uranium magnetic moment.

The spin-polarized scalar relativistic LSDA calculations [see Figs. 9(a) and 9(b)], performed to make the closest comparison with Gasche *et al.*⁴ provide the spin magnetic moments of $M_S(U) = 1.84 \mu_B$, $M_S(Pt_1) = -0.03 \mu_B$, $M_S(Pt_2) = -0.05 \mu_B$, $M_S(Al) = -0.01 \mu_B$, and $M_S(\text{interstitial}) = 0.25 \mu_B$ in the interstitial region of the UPtAl crystal. The total spin magnetic moment $M_S = 2.00 \mu_B$ is more than 50% higher than the LMTO-ASA value of $1.31 \mu_B$. Such a discrepancy between the two DFT calculations suggests an importance of the general-potential band-structure treatment of the magnetic properties in UPtAl.

Next we investigated the effect of the spin-orbit coupling (SOC). The most prominent effect of SOC is found for the U $5f$ states, where the splitting according to the total angular momentum is clearly developed [see Fig. 9(c)]. An almost 0.5 eV increase of the bandwidth due to SOC is obtained also for Pt $5d$ states. Finally, we performed spin-polarized LSDA calculations including SOC. The combined effect of the spin-polarization and SOC influences both occupied and unoccupied DOS from -1.5 eV up to 2.5 eV [see Fig. 9(d)]. Therefore a significant relation between magnetic and bulk

TABLE II. Angular decomposition of the LAPW valence charge density in the atomic spheres for UPtAl. INT is the charge in the interstitial region per one formula unit of UPtAl. $Q_i(\text{GS})$ is the total charge for the fully self-consistent calculations. $Q_i(\Sigma)$ is the total charge obtained from superposition of neutral atomic densities.

UPtAl	Q_s	Q_p	Q_d	Q_f	$Q_i(\text{GS})$	$Q_i(\Sigma)$
U	2.187	5.751	1.070	2.461	89.485	89.771
Pt_1	0.681	6.443	7.535	0.023	76.686	76.618
Pt_2	0.661	6.432	7.547	0.022	76.665	76.597
Al	0.736	6.779	0.132	0.021	11.674	11.807
INT					15.490	14.434

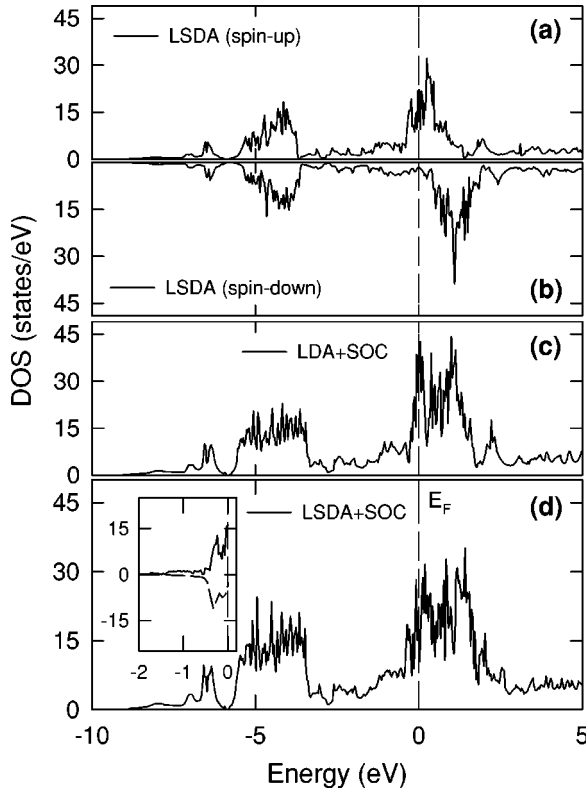


FIG. 9. Calculated scalar relativistic total spin-up (a) and spin-down (b) DOS curves assuming ferromagnetic arrangement of uranium moments. The nonmagnetic and spin-polarized DOS curves for UPtAl including SOC interaction are shown in (c) and (d) panel, respectively. The spin (full line) and orbital (dashed line) magnetic moment projected DOS are shown in the inset of figure (d).

properties can be expected. In Fig. 10, we show the DOS curves of the projected relativistic $j=5/2$ and $j=7/2$ states and the projection to the majority- and minority-spin states. It is visible that the occupied $j=5/2$ states are dominated by majority spin states but there is some admixture of minority states. Our result again demonstrates the fact that the exchange interaction energy is comparable to the SOC. Therefore, we suggest that the rather low value of the energy gap Δ derived from our specific heat and resistivity measurements (see Sec. III) originates from averaging over the magnetic excitations, which reveal at the same time the large anisotropy and the pronounced dispersions over the various directions in the Brillouin zone.

The value of DOS at the Fermi level is $N(E_F)=16$ states/eV which corresponds to $\gamma_{\text{band}}=13$ mJ mol⁻¹ K⁻². Our experimental specific-heat value is $\gamma_{\text{exp}}=65$ mJ mol⁻¹ K⁻², that points to an enhancement factor $\lambda=4$; λ is defined by the expression $\gamma_{\text{exp}}=\gamma_{\text{band}}(1+\lambda)$. This total enhancement is most likely due to electron-phonon coupling and moderate many-body enhancements. This argues for moderate correlations inside the narrow $5f$ bands of UPtAl compound. Including SOC and assuming a ferromagnetic arrangement of uranium magnetic moments aligned along c axis, as observed experimentally, the spin moments $M_S(\text{U})=1.63 \mu_B$, $M_S(\text{Pt}_1)=-0.02 \mu_B$, $M_S(\text{Pt}_2)=-0.03 \mu_B$ and the orbital moments $M_L(\text{U})=$

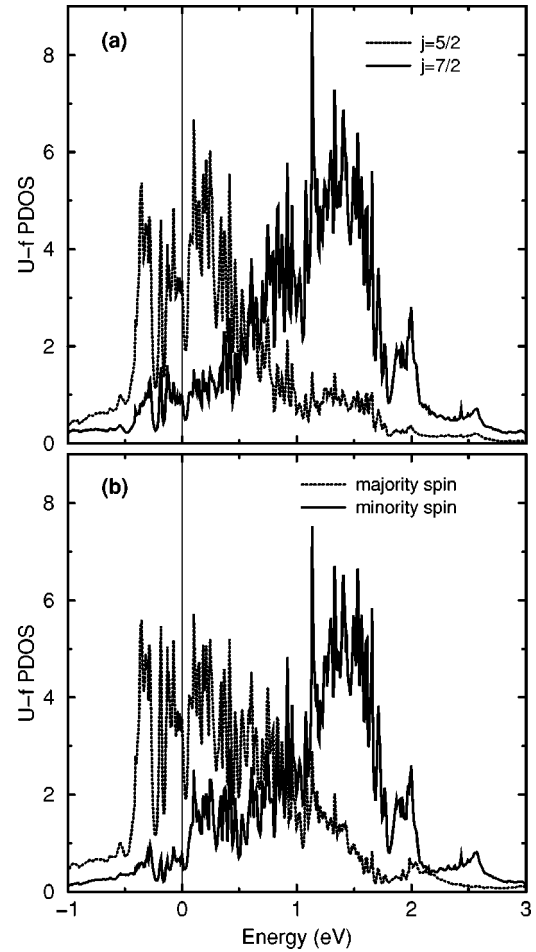


FIG. 10. Calculated relativistic $j=5/2$ (full line) and $j=7/2$ (dashed line) states and projection to the majority (dashed line) and minority (full line) spin states.

$-2.06 \mu_B$, $M_S(\text{Pt}_1)=0.01 \mu_B$, $M_S(\text{Pt}_2)=-0.02 \mu_B$, have been obtained. These our values are again rather different comparing to values calculated by LMTO-ASA method by Gasche *et al.* (see Ref. 4, table 4). We also apply our new modified code AVERX in order to calculate the orbital-magnetic-moment projected DOS. The orbital-magnetic-moment projected DOS originates from a relatively narrow energy region below the Fermi level comparing with the spin-up and spin-down DOS curves [see Figs. 9(a), 9(b), and inset of Fig. 9(d)]. The calculated total uranium moment $M_U(\text{U})=0.43 \mu_B$ can be compared with our neutron-diffraction value of $1.31 \mu_B$, which points to the importance of the orbital polarization effects,²¹ which was not included in our current band structure calculations. On the other hand, the recent x-ray magnetic circular dichroism study provides $M_L(\text{U})=-2.36 \mu_B$ (Ref. 22) that is 15% larger than our value $M_L(\text{U})=-2.06 \mu_B$. This fact suggests the importance to perform polarized neutron diffraction on single crystal, which should enable one to resolve the spin and orbital part of uranium magnetization density directly.

V. CONCLUSIONS

In conclusion, we have studied main features of electronic structure and magnetism in UPtAl both experimentally and

by *ab initio* band structure calculations. The neutron diffraction experiment in accord with magnetization data confirmed the ferromagnetic ordering of U magnetic moments ($\approx 1.3 \mu_B$) below $T_C=43$ K. The analysis of specific-heat data leads to a value of magnetic entropy that is reduced with respect to $R \ln 2$. This implies rather delocalized $5f$ electrons of uranium bearing the magnetic moment in this compound. Magnetic contributions both, to the specific heat and electrical resistivity can be well fitted with formulas containing exponential terms, which are frequently being associated with existence of a gap in magnetic excitation spectrum.¹⁶ The derived values of gap energy are however strikingly small in the light of the strong magnetocrystalline anisotropy in UPtAl (the anisotropy energy from magnetization data estimated to be larger than 130 K). Therefore, we propose that our small gap values originate from averaging over the magnetic excitations, which reveal at the same time the large anisotropy and the pronounced dispersions over the various directions in the Brillouin zone.

The results of *ab initio* density-functional calculations confirm the large exchange polarization of the uranium $5f$ states that competes with the spin-orbit splitting. The resulting self-consistent crystal-charge density was used to discuss the bonding mechanism in UPtAl compound. The rather large uranium spin $M_S(U)=1.63 \mu_B$ and orbital $M_L(U)=-2.06 \mu_B$ magnetic moment were calculated and com-

pared with the results obtained from previous calculations of Gashe *et al.* Rather small magnetic moments on platinum sites were calculated [$M_S(\text{Pt}_1)=-0.02 \mu_B$, $M_S(\text{Pt}_2)=-0.03 \mu_B$ and $M_L(\text{Pt}_1)=0.01 \mu_B$, $M_L(\text{Pt}_2)=-0.02 \mu_B$] and those on aluminum were found to be practically negligible.

The calculated total uranium moment $M_t(U)=0.43 \mu_B$ is still considerably smaller than the experimentally determined values from magnetization and neutron-diffraction measurements ($\approx 1.3 \mu_B$), which points to the importance of the orbital polarization effects,²¹ that were not included in our current band structure calculations. On the other hand, the recent x-ray magnetic circular dichroism study provides $M_L(U)=-2.36 \mu_B$,²² which is 15% larger than our value $M_L(U)=-2.06 \mu_B$.

ACKNOWLEDGMENTS

The work is a part of the research program of the Joint Laboratory for Magnetic Studies of the Charles University and Academy of Sciences. Financially, it was supported by Grants No. 202/99/0184 of the Grant Agency of the Czech Republic, No. 145/2000 of the Grant Agency of the Charles University, and No. ME162 of the Ministry of Education of the Czech Republic. M.D. and J.K. thank P. Novák for fruitful discussions and help with the AVERX code.

*Present address: Hahn-Meitner-Institute, SF-2, Glienickerstr. 100, 141 09 Berlin, Germany.

†Corresponding author. FAX: +420 2 21911351. Email address: sech@mag.mff.cuni.cz

¹V. Sechovský and L. Havela, in *Handbook of Magnetic Materials*, edited by K. H. J. Buschow (Elsevier Science B.V., Amsterdam, 1998), Vol. 1, pp. 1–289.

²D. D. Koelling, B. D. Dunlap, and G. W. Crabtree, *Phys. Rev. B* **31**, 4966 (1985).

³J. A. Paixão, G. H. Lander, P. J. Brown, H. Nakotte, F. R. de Boer, and E. Brück, *J. Phys.: Condens. Matter* **4**, 829 (1992).

⁴T. Gasche, M. S. S. Brooks, and B. Johansson, *J. Phys.: Condens. Matter* **7**, 9511 (1995).

⁵E. Brück, H. Nakotte, F. R. de Boer, P. F. de Châtel, H. P. van der Meulen, J. J. M. Franse, A. A. Menovsky, N. H. Kim Ngan, L. Havela, V. Sechovský, J. A. A. J. Perenboom, N. C. Tuan, and J. Šebek, *Phys. Rev. B* **49**, 8852 (1994).

⁶A. V. Andreev, N. V. Mushnikov, T. Goto, and V. Sechovský, *Phys. Rev. B* **60**, 1122 (1999).

⁷V. Sechovský, L. Havela, F. R. de Boer, and E. Brück, *J. Alloys Compd.* **181**, 179 (1992).

⁸A. V. Andreev, Y. Shiokawa, M. Tomida, Y. Homma, V. Sechovský, N. V. Mushnikov, and T. Goto, *J. Phys. Soc. Jpn.* **68**, 2426 (1999).

⁹N. V. Mushnikov, A. V. Andreev, A. V. Korolyov, and Y. Shiokawa, *J. Alloys Compd.* **305**, 188 (2000).

¹⁰M. S. Lehman and F. K. Larsen, *Acta Crystallogr., Sect. A: Cryst. Phys., Diffr., Theor. Gen. Crystallogr.* **A31**, 245 (1974).

¹¹J. Rodriguez-Carvajal, FULLPROF, version 3.2, JAN97, 1997.

¹²V. F. Sears, *Neutron News* **3**, 26 (1992).

¹³A. J. Freeman, J. P. Desclaux, G. H. Lander, and J. Faber, *Phys. Rev. B* **13**, 1168 (1976).

¹⁴A. V. Andreev, J. Kamarád, F. Honda, G. Oomi, V. Sechovský, and Y. Shiokawa, *J. Alloys Compd.* **314**, 51 (2001).

¹⁵D. C. Mattis, *Theory of Magnetism I* (Springer-Verlag, Berlin, 1985).

¹⁶N. H. Andersen and H. Smith, *Phys. Rev. B* **19**, 384 (1979).

¹⁷K. Prokeš, H. Nakotte, E. Brück, F.R. de Boer, L. Havela, V. Sechovský, P. Svoboda, and H. Maletta, *IEEE Trans. Magn.* **30**, 1214 (1994).

¹⁸J. P. Perdew and Y. Wang, *Phys. Rev. B* **45**, 13 244 (1992).

¹⁹P. Blaha, K. Schwarz, and J. Luitz, WIEN97, Vienna University of Technology, 1997.

²⁰T. Gasche, M.S.S. Brooks, and B. Johansson, *J. Phys.: Condens. Matter* **7**, 9499 (1995).

²¹O. Eriksson, M. S. S. Brooks, and B. Johansson, *Phys. Rev. B* **41**, 7311 (1990).

²²M. Kučera (private communication).